J Comput Aided Mol Des (2010) 24:37–47
DOI 10.1007/s10822-009-9312-1

Interactions between anti-ErbB2 antibody A21 and the ErbB2 extracellular domain provide a basis for improving A21 affinity

Liang Chang · Changhai Zhou · Man Xu · Jing Liu

Received: 17 April 2009 / Accepted: 25 November 2009 / Published online: 12 December 2009

Abstract Anti-ErbB2 antibodies are well researched for the therapy of ErbB2-overexpressing tumors. The therapeutic potential and efficacy of these antibodies are closely related to their affinities to ErbB2. Previously we reported that an anti-ErbB2 antibody A21 targeting a conformational epitope comprising several loops in ErbB2 extracellular subdomain I and II could inhibit the proliferation of ErbB2-overexpressing cancer cells in vitro and in vivo. Here we found that another structureless and non-conserved loop in subdomain I of ErbB2 extracellular domain (ECD) was important for binding to A21, and then the antigen-contact sites on A21 were determined by site-directed mutation. The loop was constructed by molecular modeling, and a new model of A21-ErbB2 complex was generated by docking using the crystal structure of the scfv A21 and the model of ErbB2 ECD with the loop built. Based on the complex model, computational design for A21 affinity improvement was performed to enhance its affinity to ErbB2. Two mutants with about 1.7-fold improvement in affinity were obtained. Our study provided a rational molecular basis for affinity improvement and mechanism investigation of A21.

L. Chang · M. Xu · J. Liu (✉)
Lab of Cellular and Molecular Immunology, School of Life Sciences, University of Science and Technology of China, 230027 Hefei, People's Republic of China
e-mail: jliu@ustc.edu.cn

C. Zhou
Hefei National Laboratory for Physical Sciences at the Microscale, School of Life Sciences, University of Science and Technology of China, 230027 Hefei, Anhui, People's Republic of China

Keywords ErbB2 · Epitope loop · Internalizing antibody · Docking · Inhibitory mechanism

Introduction

ErbB2, also known as Her2, belongs to the epidermal growth factor receptor (EGFR) family, which includes human epidermal growth factor receptors 1, 2, 3, and 4 (EGFR, HER2, HER3, and HER4) [1, 2]. Overexpression of ErbB2 is found in 20–30% of breast and ovarian tumors, and correlates with more aggressive tumors and a poorer prognosis [3–5]. Therefore, cancer therapy research has focused on the biological function of ErbB2. Unlike other members of this family, ErbB2 is thought to be an orphan receptor, as no ligands have yet been identified. Because of its constitutive extended extracellular domain, ErbB2 is the preferred heterodimerization partner for other ligand-activated ErbB receptors, and can spontaneously form signaling-competent homodimers at high concentrations [6–8]. Thus, ErbB2 plays a crucial role in the EGFR-family signaling network that governs cell proliferation and migration.

Several monoclonal antibodies (mAbs) against ErbB2 have been developed and investigated for diagnosis and therapy of ErbB2-overexpressing tumors, because of the inherent advantages of antibodies, such as target specificity, lower toxicity and longer half-life in serum than small-molecule drugs, and the capacity for multiple cytotoxic mechanisms of action. However, these antibodies showed variable effects on tumor cell growth and ErbB2 physiological functions [9–13]. Studies on antibodies against ErbB2 suggest that the efficacy and the biological function of anti-ErbB2 antibodies correlates mainly with the epitopes they target [14–16], and the inherent strengths of

antibodies correlate with affinities for the target. For therapeutic antibodies, achieving high-affinity binding means expanding detection limits, extending dissociation half-times, decreasing drug dosages and increasing drug efficacy. Many techniques are reported to improve antibody affinity, such as chain shuffling and phage display. Compared to other techniques, computational design as a method to improve antibody affinity shows higher efficiency and lower cost [17–19].

In a previous study we reported that the tumor-inhibiting anti-ErbB2 monoclonal antibody A21 recognizes a conformational epitope that includes several loops in the ErbB2 extracellular subdomain I and II [20, 21]. Functional assays showed that the affinity of A21 for its target was much lower than Herceptin, a recombinant humanized version of the anti-ErbB2 monoclonal antibody 4D5 that is used to treat patients with ErbB2-overexpressing breast cancer, but that the internalizing ability of A21 was much higher than 4D5 [22, 23]. Molecular modeling of the A21-ErbB2 complex was performed using the crystal structures of the single chain antibody scA21 (PDB code: 2GJJ) and ErbB2 ECD (PDB code: 1S78) [21]. The 100–112 fragment from the N-terminus of ErbB2 ECD was a flexible loop whose crystal structures were not resolved. We found that the epitope recognized by A21 was on the subdomains I and II of the ErbB2 ECD that included this loop fragment. The model of the complex was in good agreement with alanine-scanning results from an earlier study [21], but these did not include the flexible loop. Moreover, the antigen-contact sites (hotspots) on A21 were not confirmed experimentally. To precisely explain the relationship of the physiological functions to the A21 epitopes, and improve its affinity to create a more effective drug, the role of loop 100–112 was reevaluated. Binding hotspots on A21 were determined by site-directed mutatagenesis. Based on these results, a new model of the ErbB2-antibody complex was constructed that included this loop, and the interaction between A21 and ErbB2 was refined. The new model was used in computational designs for improving A21 affinity. A theoretical model of internalization, and an inhibitory mechanism for A21 were proposed. These results provided a rational molecular basis for research on the A21 mechanism, and a starting point for engineering to generate a new type anti-ErbB2 antibody.

Materials and methods

Vectors, antibodies and reagents

The chimeric antibody chA21 and single chain antibody scA21 were prepared as described [20, 21, 23]. The vector pSectagB containing the cDNA of the full-length human ErbB2 extracellular domain, and the vector pCANTAB-5E containing the cDNA of scA21, were constructed in our lab.

Mutagenesis scan using the GST-fusion expression system

Vector construction and expression of the ErbB2 ECD 1–192 fragment with site-directed mutations in loop 100–112, including ala-scanning and two deletion mutations were performed as described [21]. The half-maximal binding concentrations (EC50) of variants were measured in two steps by ELISA (see below). The relative binding activity was estimated by dividing the EC50 of each variant by that of the wildtype GST-ErbB2 1–192 fragment.

Identifying A21 hotspots

Construction of mutant vector

The vector pCANTAB-5E containing the cDNA of scA21 was used as the template. Site-directed mutagenesis was performed using the TaKaRa MutanBest Kit (TaKaRa), according to the manufacturer's directions.

Expression of the scA21 variants

Mutant vectors were transformed into the strain HB2151. A single clone was cultured in 50 mL 2× YT-AG (2× YT with 100 μg/mL ampicillin and 2% glucose) to a cell density of 0.3–0.4 OD_{600} and induced in 50 mL 2× YT-AI (2× YT with 100 μg/mL ampicillin and 1 mM IPTG)for 3–4 h at 30 °C with shaking at 250 rpm. Cells were collected by centrifugation (1,500×*g*, 20 min, 4 °C), suspended in 1 mL of ice-cold 1× TES (0.2 M Tris/HCl, 0.5 mM EDTA, 0.5 M sucrose) and added to 1.5 mL of ice-cold 0.2× TES. Cell suspensions were kept on ice for 30 min, then clarified by centrifugation (12,000×*g*, 10 min, 4 °C). The supernatants contained the soluble scA21 variants.

Relative affinity determination of variants by ELISA

ELISA plates were coated with threefold serial dilutions of the supernatants and incubated overnight at 4 °C before blocking with 1% nonfat milk. Mouse anti-Etag antibody was added into the plate and incubated for 1 h. HRP-conjugated goat anti-mouse antibody was added for 1 h to quantify the relative expression level of each mutant. ELISA plates were coated with 1 μg/mL ErbB2 1–192 fragment in PBS overnight at 4 °C. A twofold serial dilution of the supernatants with normalized expression level were added for 1 h. Mouse anti-Etag antibody was added

for 1 h. HRP-conjugated goat anti-mouse antibody was added for 1 h to detect binding of the mutants. The EC50 of each mutant was calculated from the binding curves, and relative affinity was estimated by dividing the EC50 of each mutant by the EC50 of wild-type scA21.

Loop modeling and molecular docking of ErbB2 1–192 fragment

The crystal structure of the ErbB2 ECD subdomain I-III (PDB code: 2A91) [24] was selected as the template for homology modeling of the ErbB2 1–192 fragment. The fragment with loop 100–112 was modeled by MODELLER [25]. All possible structures of this loop were built during loop optimization. Energy minimization was carried out by 1,000-step steepest descent and 200-step conjugate gradients.

Docking with large-scale loop movement was performed as described by Wang [26]. The rigid section in the 1–192 fragment model (without loop 98–114) and the crystal structure of scA21 (PDB code: 2GJJ) were used for rigid-backbone docking by ZDock [27]. The contact and blocking residues of each structure identified by site-directed mutation were used to filter the docking models. The flexible loop was rebuilt and refined in docking models and the final model generated by redocking with loop rebuilding.

Computational design of single mutations for improving A21 affinity

The free energy of protein complexes (ΔGcomplex) and uncomplexed free structures (ΔGfree) was calculated as described by Pokala and Handel [18]. For single mutation designs, all CDR residues were changed into the other 19 amino acids, excluding proline and cysteine. Conformations of backbone atoms were kept fixed, and side-chains were represented as discrete rotamers. Rotamers were optimized using a genetic algorithm to find the lowest energy conformation for both the complexed and free states of proteins. The side-chains of mutant residues and their neighbors (side-chains within 7 Å) were allowed to move during rotamer optimization.

The binding energy (ΔGbinding) was defined as:

$$\Delta G\text{binding} = \Delta G\text{complex} - \Delta G\text{free} \quad (1)$$

The ΔΔGcomplex and ΔΔGbinding were used for evaluation of complex stability as follows:

$$\Delta\Delta G\text{complex} = \Delta G\text{MUTcomplex} - \Delta G\text{WTcomplex} \quad (2)$$

$$\Delta\Delta G\text{binding} = \Delta G\text{MUTbinding} - \Delta G\text{WTbinding} \quad (3)$$

The energy functions contained van der Waals, coulombic electrostatics, torsional energies, and the solvation free energy, which was calculated using a variant of the generalized Born model and a hydrophobic SASA-dependent term [17]. The relative affinity of the designed mutations was measured as described above.

Results

Determining the role of ErbB2 loop 100–112 in binding to A21

The loop 100–112 mutants of ErbB2 were created, and the binding assay was performed on mutants as described in Materials and Methods. The binding curves of several mutants are shown in Fig. 1 and the complete scanning data are in Table 1. These results showed that sites located in the middle and rear of the loop, such as T105, P106,

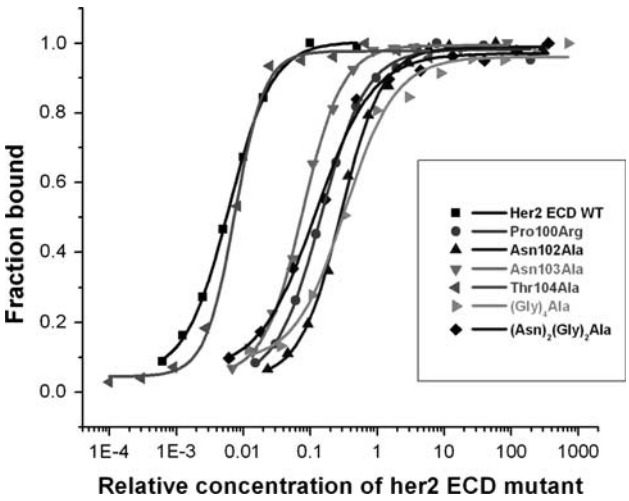

Fig. 1 Binding of wildtype and variants of ErbB2 ECD to chA21. Experimental binding curves, from *left* to *right*: wildtype, T104A, N103A, N2G2A, P100R, N102A, G4A. The X-coordinate is the relative concentration of the ErbB2 ECD mutant, as previously described [21]. The Y-coordinate is the normalized OD_{490} by ELISA

Table 1 Relative binding activity of loop 100–112 variants

Mutation[a]	Relative activity (%)	Mutation	Relative activity (%)
WT	100		
P100R	**2.0**	P106A	95
L101A	100	T108A	85
N102A	**1.1**	S111A	76.9
N103A	**6.2**	P112A	76.2
T104A	83.4	**G_4A**	**0.8**
T105A	95	**N_2G_2A**	**2.2**

[a] Mutations whose binding activity loss above tenfold are shown in bold

T108, S111 and P112, did not influence A21 binding. In contrast, mutations in the residues at the front of the loop, including P100R, N102A and N103A, showed a 100-fold decrease from the wildtype, in binding activity. The mutations L101A and T104A, also located in the front of the loop, did not show significant binding decreases. These results indicated that the front part of the loop is involved in interaction with A21, and the rear part of the loop does not affect interaction. P100, located in the beginning of the loop, appears to be critical for loop conformation, and N102 and N103 appear to be be important for A21 binding.

Two loop deletion mutations were constructed and named G4A and N2G2A, in which the amino acid sequences GGGGA and NNGGA, respectively were substituted for the 102–110 fragment of ErbB2. These two mutations had shortened flexible loops that did not influence the entire ECD structure, but led to significant loss of binding. The binding of the N2G2A mutant was about threefold higher than that of G4A mutant. Previously A21 was found to recognize a conformational epitope including several critical, spatially close residues, including D143, H171, P172 and E185. In G4A and N2G2A mutations, the loop 102–110 was shortened and N102 and N103 were pulled away from other epitope residues, disrupting binding. The significant decrease in binding activity indicated the importance of the entire loop for A21 binding, and that showed that N102 and N103 were critical residues in the loop.

Identifying the antigen-contact sites (hotspots) on A21

To investigate the interaction between A21 and ErbB2, binding hotspots in A21 were identified by a series of site-directed mutants of scA21. The mutation sites were selected from each complementary-determining region (CDR) loop, except for L2, based on the previous model of the antigen–antibody complex. The relative affinities of the mutants are shown in Table 2. All mutations of aromatic amino acids, including Y31A, Y38A in L1, Y100A in L3, F33Y in H1, Y55A in H2, Y102D, Y105W in H3, led to substantial decreases in affinity, of 10- to 100-fold,. The size of certain sites, such as the T57W mutant, might also have significantly influenced binding to ErbB2. Other conservative mutations, however, such as N33M on the light chain and N101D/Q on the heavy chain, had little effect on binding by A21. These results indicated that seven aromatic amino acids on the five CDRs contacted the antigen directly, and other amino acids made weak contacts with the antigen. According to the crystal structure of scA21, the seven aromatic amino acids contributed about 50% of the antigen-combined surface of A21 and formed the core of the A21 paratope.

Table 2 Relative affinity of the mutations of A21

Mutation on light chain	Relative affinity[a] (%)	Mutation on heavy chain	Relative affinity (%)
Y31A	3.5	F33Y	10
N33M	96.9	Y55A	1.7
N34A	70	T57W	5.2
Y38A	2.2	N101D, Q	70.5, 43.7
Y100A	6.4	Y102D	1
		Y105W	8.5

[a] The affinity of wide-type scfv A21 for ErbB2 is normalized as 100%

Loop modeling and docking of ErbB2 1–192 fragment

The intact structure of the ErbB2 1–192 fragment was modeled by homology modeling. The conformational structure of loop 100–112 was optimized and the intact structure was evaluated as described in Materials and Methods. All possible conformational structures of the loop were generated to build a loop database. Considering that most of the epitope residues located in the rigid fragment of ErbB2, we performed rigid-backbone docking for A21 and the critical eitope residues. So the crystal structures of both A21 and the rigid fragment of ErbB2, and the contact and blocking residues of each protein that had been identified experimentally (Table 3), were used for rigid backbone docking by Zdock.

The flexible loop was rebuilt on 17 simulated complex models based on the loop database. The models with a rebuilt loop were examined and those in which the loop did not participate in binding to A21 were excluded. In the remaining six models, A21 and ErbB2 interacted with each other in a similar pattern. Based on these models, molecular docking with the rebuilt loop was carried out by HEX4.5, and the rotation of conformations of A21 and ErbB2 were restricted. For each models, the energy of the mutation residues on the loop were considered as critical parameter and compared with the results of mutagenesis scanning. Then the complex models highly consistent with the results of the experimental mutation were ranked by the free energy (ΔGcomplex) and the binding energy (ΔGbinding). The model was selected with both lowest free energy and

Table 3 Contact and blocking residues identified by experimental method

Molecule	Contact residues	Blocking residues
ErbB2	D143 R166 R168 H171 P172 E185	T164 M176-R181
A21	$Y31^{L}$ $Y38^{L}$ $Y100^{L}$ $F33^{H}$ $Y55^{H}$ $T57^{H}$ $N101^{H}$ $Y102^{H}$ $Y105^{H}$	–

low binding energy. In this model, the residues located in the interaction interface matched most of the contact residues determined by mutagenesis scanning or computer prediction (Table 4).

Unlike the previous model, the epitope was located on the top side of ErbB2 (Fig. 2a). It was mainly composed of two loops, one of which was loop 100–112 in subdomain I and another of which was loop 164–174 at the junction region of subdomain I and II. The binding interface is shown in Fig. 2b. Two successive residues, H171 and P172, were located at the center of the epitope, and were close to another two successive residues, N102 and N103, when loop 100–112 bent upwards toward the center of epitope after binding to A21. Furthermore, D143 and E185 also interacted directly with A21. As expected, with the exception of L2, the six CDRs from A21 showed direct contact with ErbB2. L2 played a major role in interactions between the light and heavy chains of A21, maintaining structural stability. The A21 paratope was composed of seven aromatic amino acids, including Y31, Y38, Y100 in the light chain and F33, Y55, Y102, Y105 in the heavy chain. Other residues also showed interactions with ErbB2, including N33, N34, K36 in L1, H50, S52, S54, T57 in H2 and N101 in H3. Although the hotspots in this model were similar to those in the previous model, the interaction pattern was different. The inclusion of stability analysis from alanine-scanning of the interface residues that created mutants on the epitope loops of ErbB2, and hotspots on A21 could explain the affinity changes in the new model (Table 4). This model should provide valuable information for designing site-directed mutations to improve A21 affinity, and for investigating the molecular mechanism of A21 function.

Improving the affinity of A21 by computational design and experimental testing

Computational design for improving the affinity of A21 was performed based on the new antigen–antibody complex model. The stability of substitutions was evaluated as described in Materials and Methods. Substitutions beneficial for the structural stability of the antigen–antibody complex ($\Delta\Delta G$binding < -0.2 and $\Delta\Delta G$complex < 0) were selected. Most substitutions could not bind more tightly than wildtype A21 ($\Delta\Delta G$binding > 0). In particular, substitutions of aromatic amino acids showed obviously decreased complex stability (data not shown). Computational design on L1 is shown in Table 5. Two mutations,

Table 4 Binding energy and binding activity of mutations of interfacial residues in A21-ErbB2 complex model

Mutation	$\Delta\Delta G_{binding}$ (kcal/M)	Relative activity (%)	Mutation	$\Delta\Delta G_{binding}$ (kcal/M)	Relative activity (%)
(a) Alanine-scanning of interfacial residues on ErbB2 [21]					
L101A	0.00	100	S167A	−0.24	115
N102A	1.64	1.1	R168A	0.00	0.11
N103A	1.69	6.2	C170A	−0.21	–
T104A	0.24	83.4	H171A	1.66	0.51
D143A	2.15	2.34	P172A	4.94	0.12
D163A	−0.13	–	C173A	0.00	–
T164A	0.09	105	S174A	0.46	61.7
N165A	0.58	66	E185A	1.69	78
R166A	6.59	2.45	S187A	0.15	44
Mutation On L chain	$\Delta\Delta G_{binding}$ (kcal/M)	Relative affinity (%)	Mutation On H chain	$\Delta\Delta G_{binding}$ (kcal/M)	Relative affinity (%)
(b) Alanine scanning and mutations of interfacial residues on A21					
Y31A	2.56	3.5	T30A	0.25	–
N33A	0.58	–	F33Y	Huge[a]	10
N34A	0.35	70	H50A	0.88	–
Q35A	0.60	–	S52A	1.29	–
K36A	0.37	–	S54A	1.00	–
Y38A	1.33	2.2	Y55A	3.47	1.7
N99A	0.01	–	T57A	0.33	–
Y100A	3.31	6.4	T59A	0.01	–
W102A	0.25	–	N101A	1.64	–
			Y102D	4.28	1
			Y105W	Huge[a]	8.5

[a] The value of $\Delta\Delta G_{binding}$ which is bigger than 10 kcal/M is signed as 'huge'

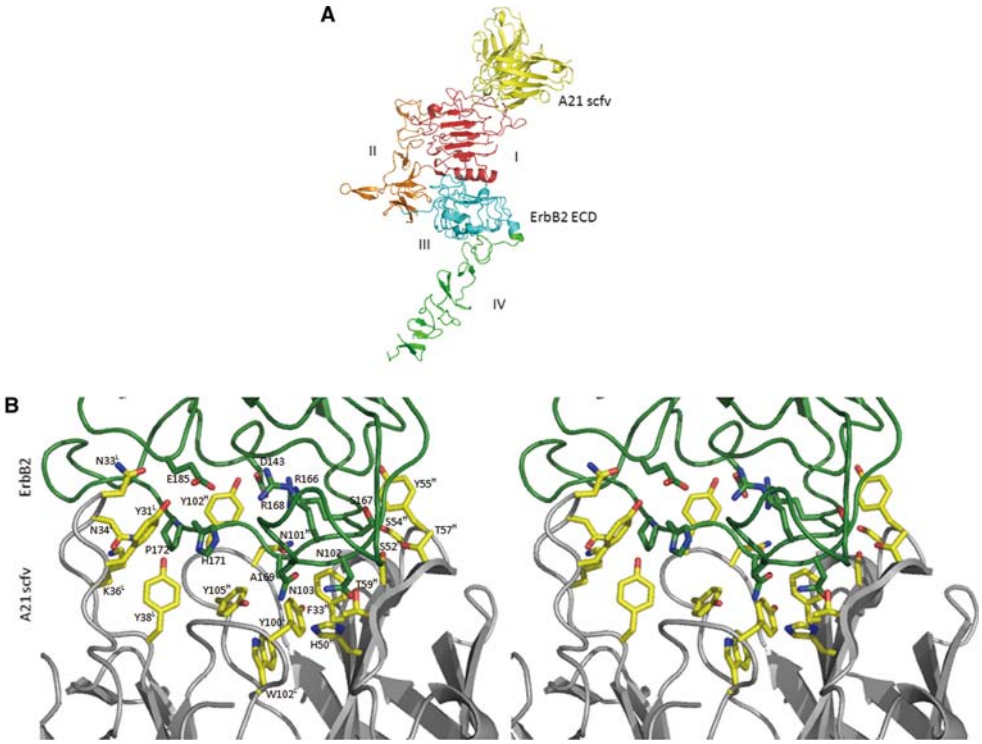

Fig. 2 Model of the scA21 and ErbB2 ECD complex. **a** Overview structure of the complex. ErbB2 ECD subdomain I (*red*), II (*orange*), III (*cyan*), IV (*green*), and scA21 (*yellow*) are shown. **b** The binding interface of the complex in stereo. The predicted contact residues are labeled out with carbon atoms from their side chains. These residues include Y31, N33, N34, K36, Y38, Y100 on the light chain, F33, S52, S54, Y55, T57, T59, N101, Y102, Y105 on the heavy chain of A21 (*yellow*) and N102, N103, D143, R166, S167, R168, A169, H171, P172, E185 on ErbB2 ECD (*green*). This figure was generated by PyMOL v0.99

^{L}N33K and ^{L}K36F, exhibited ~1.7- and 1.4-fold improvements, respectively. Other substitutions showed no improvement or even impaired the binding, with decreases of three to fourfold affinity. In the complex model, ^{L}N33K increased electrostatic interaction with E185 on ErbB2, and ^{L}K36F increased hydrophobic and van der Waals interactions. In addition, other substitutions in other CDRs exhibited weak effects on affinity ($-0.2 < \Delta\Delta G\text{binding} < 0$, data not shown).

Discussion

We hypothesize that the epitopes recognized by anti-ErbB2 antibodies are related to their biological functions. As reported previously, the internalizing ability of A21 is much higher than 4D5, but its affinity for ErbB2 is lower than that of 4D5 [23]. In our previous study, a structural model of the A21-ErbB2 complex was established to investigate the mechanisms of A21 [21]. Although this model was in good agreement with the experimental results from mutations of several sites on the ErbB2 ECD, some ambiguities remained. First, the flexible loop 100–112 in subdomain I of the ErbB2 ECD could not be analyzed, because no crystal structure could be obtained. Second, in the previous model, some antigen-contact residues on A21 were not within the CDRs or the known contact regions.

In this study, we showed that the conformational structure of loop 100–112 of ErbB2 was important for A21 binding, and that this epitope loop acted allosterically during binding to A21. In other studies [28, 29], these characteristics were due to the flexibility of the epitope loop and induced-fit effects of the antibody. Two residues on this loop, N102 and N103, and several surface-exposed residues that were previously identified as epitope residues, including D143, R166, R168, H171, P172 and E185, composed the whole epitope. Another two residues, R116 and Q138, were hidden under the molecular surface of loop 100–112, so that they could not directly contact A21, but they also were found to be important for loop 100–112 conformation. Therefore, the decreased binding of R116A and Q138A mutations might be due to conformational changes of loop 100–112, rather than effects on direct binding to A21. Results presented here identify the epitope

Table 5 Computational design in L1 for A21 affinity improvement

Mutation	$\Delta\Delta G_{binding}$ (kcal/M)	Relative affinity (%)	Mutation	$\Delta\Delta G_{binding}$ (kcal/M)	Relative affinity (%)
Y31K	−0.22	30.6	N33K	−0.50	173
Y31W	−2.54	105	N33M	−2.86	96.9
Y31H	−1.16	28.8	K36F	−3.13	140

more exactly, to include N102, N103, D143, R166, R168, H171, P172 and E185. These residues are in the ErbB2 ECD subdomain I and II, on the opposite side of the subdomains II and IV that are critical for receptor dimerization. Thus, A21 binding should not influence normal dimerization of ErbB2. Furthermore, this highly flexible loop epitope might be the reason for the low affinity of A21 and be related to its internalization characteristics.

Compared to the previous model, the new model presented here not only considered the extra epitope loop 100–112, but was superior in elucidating the interaction pattern between A21 and ErbB2. Identified hotspots of A21 included six Tyr residues and one phe residue, which played major roles in ErbB2 recognition. Consistent with these results, many studies have shown that aromatic residues, especially Tyr and Trp, are frequently found at the center of interaction sites and make more favorable contributions to binding than other residues [30–38]. In contrast to Tyr, Phe usually has much less significance. However, Phe was superior to Tyr at $^{H}33$ of A21. According to the new model, this is the result of steric exclusion between the hydroxyl group on the sidechain of ^{H}Y33 and backbone atom of R168 on ErbB2. ^{L}N33K and ^{L}K36F, two mutations with improved affinity, contributed of two electrostatic mechanisms from single mutations: one was the addition of a charged residue at the periphery of the antibody–antigen interface; the other eliminated a poorly satisfied polar group.

Although the interaction pattern between the flexible loop 102–110 of ErbB2 and A21 could not be simulated exactly in this model, it still provided useful structural information for improving affinity. For example, L1 and H2 are potential target regions for affinity improvement because many residues in these two loops contacted the antigen directly. H3, a common target region for affinity improvement, appears irreplaceable in the new model because it contains two important Tyr residues. Further improvements using multiple mutations should give improved effects. In conclusion, the complex model showed rationality and feasibility as a model for molecular reconstruction of A21.

At present, anti-ErbB2 antibodies involved in clinical therapy can be divided two types: (1) antibodies used to directly inhibit the proliferation of ErbB2-overexpressing cancer cells; (2) internalizing antibodies used to transfer drugs to target cells. The inhibitory antibodies often act through two mechanisms, including downregulating active levels of ErbB2 or downstream signaling molecules, and inducing cell cycle arrest. 4D5 and 2C4, two typical inhibitory antibodies whose functional mechanisms are well known, recognize crucial sites for receptor dimerization in subdomain II and IV respectively [8, 39, 40]. The functional mechanisms and the epitopes of the internalizing antibodies are not well characterized however, and there seems to be no correlation between inhibitory and internalizing activity [41]. An antibody, L26, with both inhibitory and internalizing activity has been reported to downregulates ErbB2 levels by ubiquitin-dependent protein degradation, but its epitope is not known [42]. Previously, A21 has been shown to have bivalency-dependent inhibitory activity and bivalency-independent internalizing activity [21, 23]. Insights into the correlation between the function and binding site of A21 should have profound implications for understanding the molecular functional mechanism of similar antibodies.

ErbB2 is reported to be impaired in endocytosis and able to inhibit internalization of EGF-bound EGFR [43, 44]. Homoclusters of ErbB receptors have been found on the surface of ErbB-expressing cells in the absence of ligand [45, 46], and the formation of these inactive homoclusters might be driven by the transmembrane domains of the receptors [47]. In the presence of ligands, the ligand-bound ErbB ECDs undergoes conformational changes and exposes the receptor dimerization regions in subdomain II and IV to form back-to-back dimers [48, 49]. Subsequently, the intracellular tyrosine kinase domains dimerize in certain patterns to activate and phosphorylate each other [50]. The back-to-back ErbB dimers were examined by crystallological method and widely accepted as the pattern of ligand-induced dimerization. However, this model does not sufficiently explain the multiple-affinity states of EGFR [51]. Recently, Stephen et al. [52] showed the relationship between two classes of EGFR with diverse affinities for EGF and two patterns of dimerization. One pattern was back-to-back dimers and the other was head-to-head dimers, in which the ECDs had a flat orientation on the membrane that involved contacts between subdomains I and III. By aligning the structures and sequences of ErbB ECDs, we deduced that ErbB3 and ErbB4 could form head-to-head dimers, but the non-conserved loop 100–112 in ErbB2 subdomain I could interfere directly with head-to-head dimerization or could mediate the combination between ErbB2 and certain proteins in a way that restrained the swing of the ECD or restricted the distribution of ErbB2 (Fig. 3). Interestingly, A21 recognized this loop and might eliminate the influence on head-to-head dimerization of ErbB2.

Endocytosis is required for the regulation of membrane-bound proteins such as EGFR. All ErbB receptors other than EGFR are reported to be endocytosis-impaired [53] and the sequences of ErbB intracellular domains (ICD) are the crucial factor for endocytosis [53, 54]. However, internalizing antibodies against ErbB ECD indicate that conformation changes in ECD could influence the ICD.

According to the role of rotational positioning in receptor signaling [55], we propose a model for the internalizing and inhibitory mechanism of A21 (Fig. 4). In the presence of

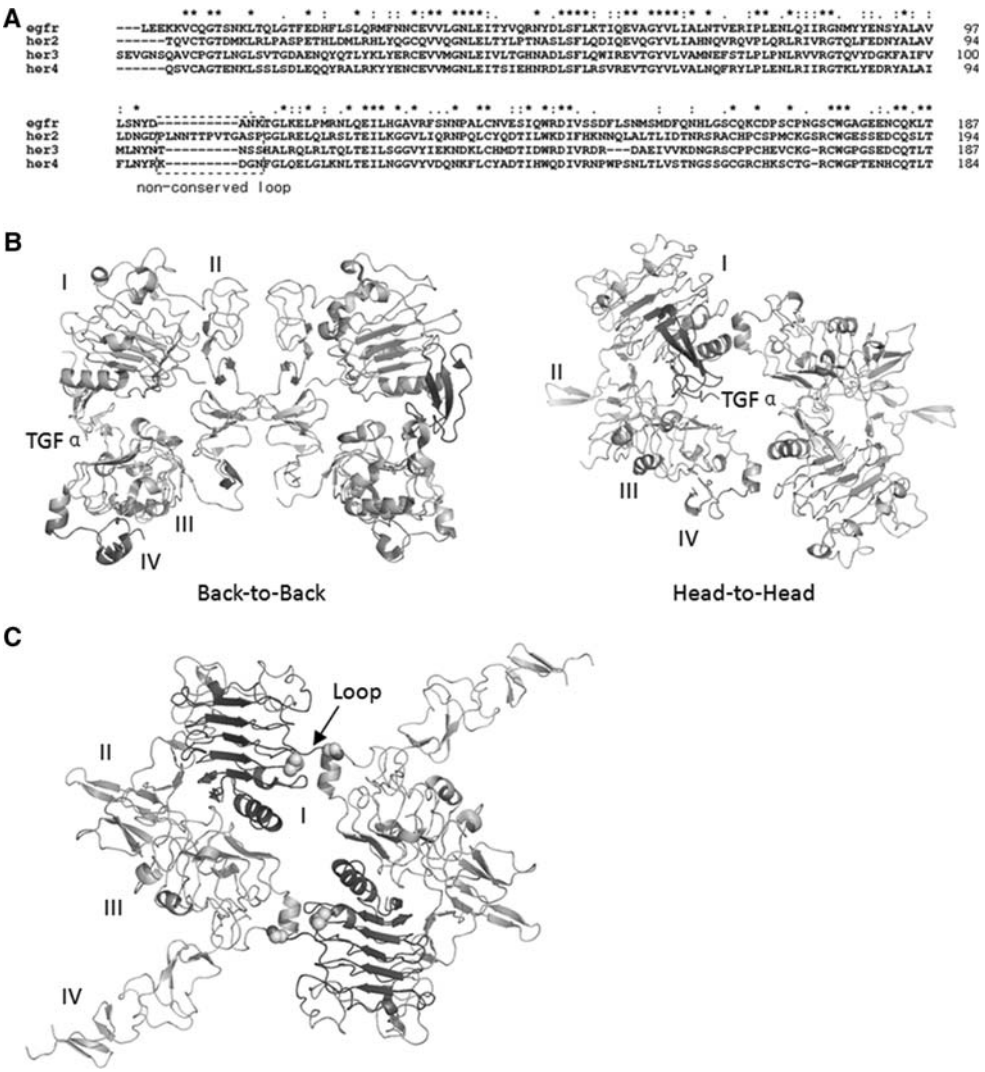

Fig. 3 Sequence alignment of ErbB receptors and two patterns of ErbB receptors dimerization. **a** The alignment of ErbBs ECD subdomain I and part of subdomain II were generated in ClustalX. (*) Residues are conserved; (:) and (•) residues are similar; gaps are denoted by a *dash* (-). **b** The two TGFα-EGFR dimerization patterns [49]: back-to-back (*left*, *side view*) and head-to-head (*right*, *top view*). **c** Model of ErbB2 head-to-head dimerization (*top view*): the non-conserved loop is represented by two-end stub residues shown in spheres

ligands, ligand-bound EGFR dimerizes in both the back-to-back and head-to-head patterns. In both dimerization patterns, some residues of EGFR ICD are exposed in directions suitable for serving as the docking sites for endocytosis-associated proteins that can bind as a dimer [56] and trigger endocytosis. ErbB2, however, dimerizes spontaneously. Because of the differences in amino acid sequence of EGFR ICD and ErbB2 ICD, unsuitable rotational positioning of docking sites leads to unstable combinations of downstream endocytosis-associated proteins or burying of their side-chains, with consequent low endocytosis efficiency for back-to-back ErbB2 dimers. In head-to-head dimers, the rotational positioning of docking sites does not interfere with endocytosis or the suitable exposure of the sites. However, the fact that the non-conserved loop in ErbB2 subdomain I interfered with dimerization in head-to-head pattern could explain why ErbB2 is impaired in endocytosis, and why internalization of EGF-bound EGFR is inhibited by high-level expression of ErbB2 [43, 44]. Treatment with the monovalent antibody scA21 eliminates the interference and induces head-to-head dimerization and subsequent internalization of ErbB2. Nevertheless, endocytosis induced by scA21 had no effect on cell proliferation, or ErbB2 phosphorylation and downregulation [21]. This suggests that the internalized receptors recycle back to the plasma membrane. In contrast, bivalent antibodies with inhibitory activity target two ErbB2 molecules and induce them to form an analogous head-to-head internalized complex. Structurally, the epitope appears to be far from the critical dimerization regions of receptor, so the ErbB2 targeted by the bivalent antibody could dimerize with additional ErbB2 molecules and form a more complex polymer of antibodies and receptors. This is similar to the protein complex recently proposed to be formed during treatment with combinations of anti-ErbB2 mAbs [57, 58], that might be internalized and downregulated through a similar mechanism. Other ErbB receptors have been proposed to be downregulated indirectly by bivalent A21, to varying

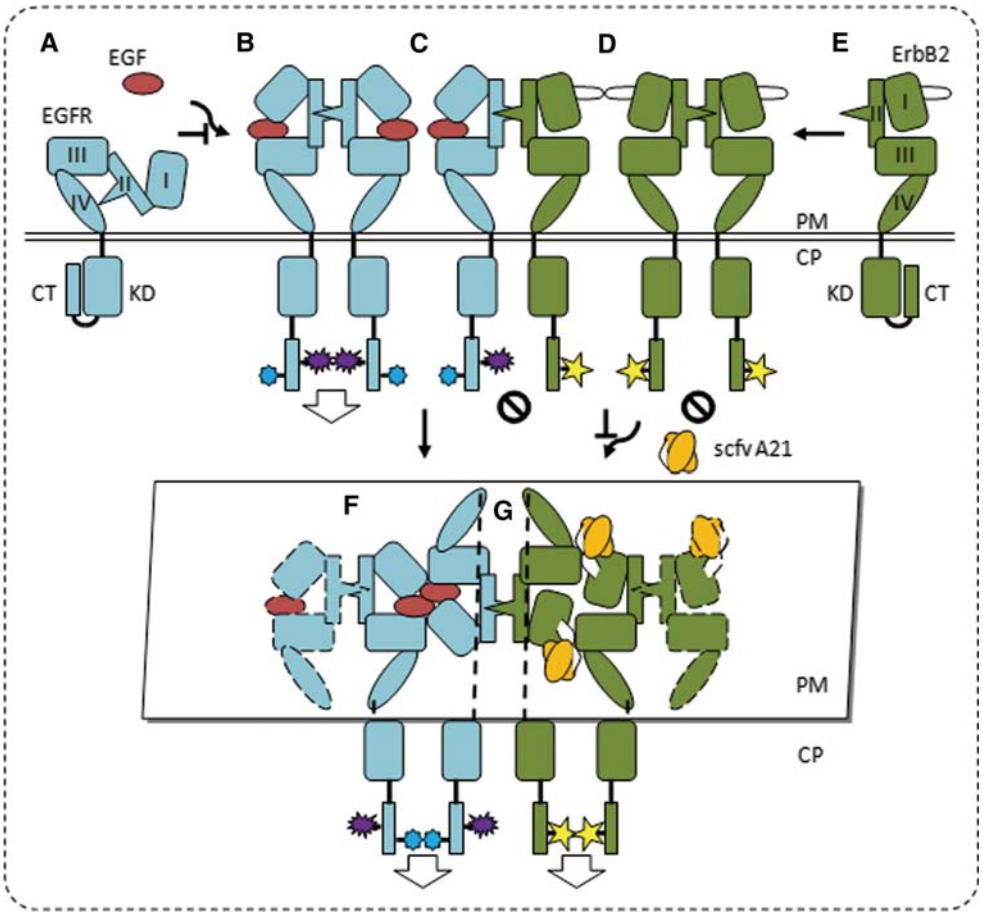

Fig. 4 Internalization mechanism of A21. The C-terminal domains (*CT*) are sheltered in the EGFR monomer (**a**) or the ErbB2 monomer (**e**). In the presence of ligands (such as EGF), the ligand-bound EGFR forms a homodimer (**b**), a heterodimer (**c**) in a back-to-back pattern, and a homodimer (**f**) in a head-to-head pattern. ErbB2 spontaneously forms a homodimer (**d**) in a back-to-back pattern, and dimerizes in a head-to-head pattern (**g**) until the addition of scA21. The dimers are internalized when the docking sites in CTs of receptors are exposed and bind as a dimer, as shown in **b**, **f**, **g**. The dimers are not internalized when the dimer of the docking sites cannot be formed (shown in **c**, **d**). The ErbB ECDs are oriented flat on plasma membrane (*PM*) (shown in **f** and **g**). *KD* kinase domain, *CP* cytoplasm

degrees that differ according to their capability to heterodimerize with ErbB2. This proposal was recently verified experimentally, confirming that bivalent A21 could downregulate EGFR and ErbB3 in SKBR3 cells (unpublished data). This implies that A21 is not only a direct inhibitor of ErbB2, but also a potential regulator of other ErbB receptors and even ErbB2-crosslinked, membrane-bound proteins.

Although anti-ErbB2 antibodies have been extensively epitope mapped, correlations between epitopes and their mechanisms are still uncertain because of insufficient crystallogical evidence. Our study implies that with advances in the technology of molecular modeling and docking, combinatorial bioinformatics methods will become a feasible, convenient and accurate approach for exploring protein–protein interactions, because we obtained intuitive structural information about targets. We showed that a non-conserved loop with unknown structure was related to ErbB2 endocytosis and could be another critical region of ErbB2, along with the dimerization regions. Research on the recognition of ErbB2 by the A21 antibody has profound implications for understanding the mechanism of antibody-induced internalization and downregulation of ErbB2. We propose that internalizing antibodies might play a greater role in ErbB2-related cancer therapy.

Acknowledgments We thank Thomas P. Garrett and Colin W. Ward for helpful discussions and the gift of the atomic coordinates of EGFR dimer. This work is supported by Hi-Tech Research and Development Program ("863" Program) of the Ministry of Science and Technology of China (no. 2006AA02A245), Specialized Research Fund for the Doctoral Program of Higher Education (no. 20060358021) and National Natural Science Fund of China (no. 30570362).

References

1. Akiyama R, Sudo C, Ogawra H, Toyoshima K, Yamamoto T (1986) The product of the human C-erbB-2 gene a 185 kilodalton glycoprefein with tyrosine kinase activity. Science 232:1644
2. Bargmann CI, Hung MC, Wwinberg RA (1986) The neu oncogene encodea an epidermal growth factor recepter-related protein. Nature 319:226
3. Carlsson J, Nordgren H, Sjostrom J, Wester K, Villman K, Bengtsson NO, Ostenstad B, Lundqvist H, Blomqvist C (2004) HER2 expression in breast cancer primary tumours and corresponding metastases. Original data and literature review. Br J Cancer 90(12):2344–2348
4. Citri A, Skaria KB, Yarden Y (2003) The deaf and the dumb: the biology of *ErbB*-2 and *ErbB*-3. Exp Cell Res 284:54–65

5. Slamon DJ, Clark GM, Wong SG, Levin WJ, Ullrich A, McGuire WL (1987) Human breast cancer: correlation of relapse and survival with amplification of the HER-2/neu oncogene. Science 235:177–182
6. Graus-Porta D, Beerli RR, Daly JM, Hynes NE (1997) ErbB-2, the preferred heterodimerization partner of all ErbB receptors, is a mediator of lateral signaling. EMBO J 16(7):1647–1655
7. Harari D, Yarden Y (2000) Molecular mechanisms underlying ErbB2/HER2 action in breast cancer. Oncogene 19(53):6102–6114
8. Cho HS, Mason K, Ramyar KX, Stanley AM, Gabelli SB, Denney DW Jr, Leahy DJ (2003) Structure of the extracellular region of HER2 alone and in complex with the Herceptin Fab. Nature 421(6924):756–760
9. Poul MA, Becerril B, Nielsen UB, Morisson P, Marks JD (2000) Selection of tumor-specific internalizing human antibodies from phage libraries. J Mol Biol 301:1149–1161
10. Baselga J, Albanell J (2001) Mechanism of action of anti-HER2 monoclonal antibodies. Ann Oncol 12:S35–S41
11. Yum LY, Robyn LW (2002) Anti-ErbB2 monoclonal antibodies and ErbB2-directed vaccines. Cancer Immunol Immunother 50:569–587
12. Lorenzo CD, Palmer DB, Piccoli R, Ritter MA, D'Alession G (2002) A new human antitumor immunoreagent specific for ErbB2. Clin Cancer Res 8:1710–1719
13. Itoh K, Inoue K, Tezuka T, Tada H, Hashimoto Y, Masuko T, Suzuki T (2003) Molecular structural and functional characterization of tumor suppressive anti-ErbB2 monoclonal antibody by phage display system. J Biochem 133:239–245
14. Xu FJ, Lupu R, Rodriguez GC, Whitaker RS, Boente MP, Berchuck A, Yu Y, DeSombre KA, Boyer CM, Bast RC Jr (1993) Antibody-induced growth inhibition is mediated through immunochemically and functionally distinct epitopes on the extracellular domain of the c-erbB-2 (HER-2/neu) gene product p185. Int J Cancer 53:401–408
15. Lewis-phillips GD, Mcmurtrey AE, Schroeder K, Fendly BM (1998) Diverse activities of anti-HER-2 monoclonal antibodies: from growth inhibition to induction of apoptosis. Proc Am Assoc Cancer Res 39:143
16. Boyer CM, Pusztai L, Wiener JR, Xu FJ, Dean GS, Bast BS, O'Briant KC, Greenwald M, DeSombre KA, Bast RC Jr (1999) Relative cytotoxic activity of immunotoxins reactive with different epitopes on the extracellular domain of the c-erbb-2 (her-2/neu) gene product p185. Int J Cancer 82:525–531
17. Pokala N, Handel TM (2004) Energy functions for protein design I: efficient and accurate continuum electrostatics and solvation. Protein Sci 13:925–936
18. Pokala N, Handel TM (2005) Energy functions for protein design: adjustment with protein–protein complex affinities, models for the unfolded state, and negative design of solubility and specificity. J Mol Biol 347:203–227
19. Lippow SM, Wittrup KD, Tidor B (2007) Computational design of antibody-affinity improvement beyond in vivo maturation. Nat Biotechnol 25:1171–1176
20. Cheng L, Liu A, Liu J (2003) Construction, expression and characterization of the engineered antibody against tumor surface antigen $P185^{c\text{-}erbb-2}$. Cell Res 13:35–48
21. Hu S, Zhu Z, Li L, Chang L, Li W, Cheng L, Teng M, Liu J (2008) Epitope mapping and structural analysis of an anti-ErbB2 antibody A21: molecular basis for tumor inhibitory mechanism. Proteins 70(3):938–949
22. Carter P, Presta L, Gorman CM, Ridgway JB, Henner D, Wong WL, Rowland AM, Kotts C, Carver ME, Shepard HM (1992) Humanization of an anti-p185HER2 antibody for human cancer therapy. Proc Natl Acad Sci USA 89(10):4285–4289
23. Hu S, Li L, Qiao J, Guo Y, Cheng L, Liu J (2006) Codon optimization, expression and characterization of an internalizing anti-ErbB2 single chain antibody in Pichia pastoris. Protein Expr Purif 47:249–257
24. Garrett TP, McKern NM, Lou M, Elleman TC, Adams TE, Lovrecz GO, Kofler M, Jorissen RN, Nice EC, Burgess AW, Ward CW (2003) The crystal structure of a truncated ErbB2 ectodomain reveals an active conformation, poised to interact with other ErbB receptors. Mol Cell 11:495–505
25. Eswar N, Webb B, Marti-Renom MA, Madhusudhan MS, Eramian D, Shen MY, Pieper U, Sali A (2006) Comparative protein structure modeling using MODELLER. Curr Protoc Bioinformatics, Chap. 5,Unit 56
26. Wang C, Bradley P, Baker D (2007) Protein–protein docking with backbone flexibility. J Mol Biol 373:503–519
27. Chen R, Li L, Weng Z (2003) ZDOCK: an initial-stage protein-docking algorithm. Proteins 52(1):80–87
28. Bhat TN, Bentley GA, Fischmann TO, Boulot G, Poljak RJ (1990) Small rearrangements in structures of Fv and Fab fragments of antibody D1.3 on antigen binding. Nature 347:483–485
29. Rini JM, Schulze-Gahmen U, Wilson IA (1992) Structural evidence for induced fit as a mechanism for antibody–antigen recognition. Science 255:959–965
30. Lo Conte L, Chothia C, Janin J (1999) The atomic structure of protein–protein recognition sites. J Mol Biol 285(5):2177–2198
31. Bogan AA, Thorn KS (1998) Anatomy of hot spots in protein interfaces. J Mol Biol 280(1):1–9
32. Chakrabarti P, Janin J (2002) Dissecting protein–protein recognition sites. Proteins 47:334–343
33. Janin J, Chothia C (1990) The structure of protein–protein recognition sites. J Biol Chem 265:16027–16030
34. Davies DR, Cohen GH (1996) Interactions of protein antigens with antibodies. Proc Natl Acad Sci USA 93:7–12
35. Livesay DR, Subramaniam S (2004) Conserved sequence and structure association motifs in antibody–protein and antibody–hapten complexes. PEDS 17(5):463–472
36. Mian IS, Bradwell AR, Olson AJ (1991) Structure, function and properties of antibody binding sites. J Mol Biol 217:133–151
37. Fellouse FA, Wiesmann C, Sidhu SS (2004) Synthetic antibodies from a four-amino-acid code: a dominant role for tyrosine in antigen recognition. Proc Natl Acad Sci USA 101:12467–12472
38. Shiroishi M, Tsumoto K, Tanaka Y, Yokota A, Nakanishi T, Kondo H, Kumagai I (2007) Structural consequences of mutations in interfacial Tyr residues of a protein antigen–antibody complex. The case of HyHEL-10-HEL. J Biol Chem 282:6783–6791
39. Franklin MC, Carey KD, Vajdos FF, Leahy DJ, de Vos AM, Sliwkowski MX (2004) Insights into ErbB2 signaling from the structure of the ErbB2-pertusumab complex. Cancer Cell 5:317–327
40. Badache A, Hynes NE (2004) A new therapeutic antibody masks ErbB2 to its partners. Cancer Cell 5:299–301
41. Neve RM, Nielsen UB, Kirpotin DB, Poul MA, Marks JD, Benz CC (2001) Biological effects of anti-ErbB2 single chain antibodies selected for internalizing function. Biochem Biophys Res Comm 280:274–279
42. Klapper LN, Waterman H, Sela M, Yarden Y (2000) Tumor-inhibitory antibodies to HER-2/ErbB-2 may act by recruiting c-Cbl and enhancing ubiquitination of HER-2. Cancer Res 60:3384–3388
43. Hommelgaard AM, Lerdrup M, van Deurs B (2004) Association with membrane protrusions makes ErbB2 an internalization-resistant receptor. Mol Biol Cell 15:1557–1567
44. Haslekas C, Breen K, Pedersen KW, Johannessen LE, Stang E, Madshus IH (2005) The inhibitory effect of ErbB2 on epidermal growth factor-induced formation of clathrin-coated pits correlates

with retention of epidermal growth factor receptor-ErbB2 oligomeric complexes at the plasma membrane. Mol Biol Cell 16: 5832–5842
45. Clayton AH, Walker F, Orchard SG, Henderson C, Fuchs D, Rothacker J, Nice EC, Burgess AW (2005) Ligand-induced dimer-tetramer transition during the activation of the cell surface epidermal growth factor receptor-A multidimensional microscopy analysis. J Biol Chem 280:30392–30399
46. Szabó A, Horváth G, Szöllosi J, Nagy P (2008) Quantitative characterization of the large-scale association of ErbB1 and ErbB2 by flow cytometric homo-FRET measurements. Biophys J 95:2086–2096
47. Mendrola JM, Berger MB, King MC, Lemmon MA (2002) The single transmembrane domains of ErbB receptors self-associate in cell membranes. J Biol Chem 277:4704–4712
48. Ogiso H, Ishitani R, Nureki O, Fukai S, Yamanaka M, Kim JH, Saito K, Sakamoto A, Inoue M, Shirouzu M, Yokoyama S (2002) Crystal structure of the complex of human epidermal growth factor and receptor extracellular domains. Cell 110:775–787
49. Garrett TP, McKern NM, Lou M, Elleman TC, Adams TE, Lovrecz GO, Zhu HJ, Walker F, Frenkel MJ, Hoyne PA, Jorissen RN, Nice EC, Burgess AW, Ward CW (2002) Crystal structure of a truncated epidermal growth factor receptor extracellular domain bound to transforming growth factor alpha. Cell 110:763–773
50. Zhang X, Gureasko J, Shen K, Cole PA, Kuriyan J (2006) An allosteric mechanism for activation of the kinase domain of epidermal growth factor receptor. Cell 125:1137–1149
51. Domagala T, Konstantopoulos N, Smyth F, Jorissen RN, Fabri L, Geleick D, Lax I, Schlessinger J, Sawyer W, Howlett GJ, Burgess AW, Nice EC (2000) Stoichiometry, kinetic and binding analysis of the interaction between epidermal growth factor (EGF) and the extracellular domain of the EGF receptor. Growth Factors 18:11–29
52. Webb SE, Roberts SK, Needham SR, Tynan CJ, Rolfe DJ, Winn MD, Clarke DT, Barraclough R, Martin-Fernandez ML (2008) Single-molecule imaging and Fluorescence Lifetime Imaging Microscopy show different structures for high- and low-affinity epidermal growth factor receptors in A431 cells. Biophys J 94:803–819
53. Baulida J, Kraus MH, Alimandi M, Di Fiore PP, Carpenter G (1996) All ErbB receptors other than the epidermal growth factor receptor are endocytosis impaired. J Biol Chem 271:5251–5257
54. Wang Z, Zhang L, Yeung TK, Chen X (1999) Endocytosis deficiency of epidermal growth factor (EGF) receptor–ErbB2 heterodimers in response to EGF stimulation. Mol Biol Cell 10:1621–1636
55. Yip YM, Novetny J, Edwards M, Ward RL (2003) Structural analysis of the ErbB2 receptor using monoclonal antibodies: implications for receptor signaling. Int J Cancer 104:303–309
56. Owen DJ, Evans PR (1998) A structural explanation for the recognition of tyrosine-based endocytotic signals. Science 282:1327–1332
57. Friedman LM, Rinon A, Schechter B, Lyass L, Lavi S, Bacus SS, Sela M, Yarden Y (2005) Synergistic down-regulation of receptor tyrosine kinases by combinations of mAbs: implications for cancer immunotherapy. Proc Natl Acad Sci USA 102(6):1915–1920
58. Ben-Kasus T, Scehchter B, Lavi S, Yarden Y, Sela M (2009) Persistent elimination of ErbB-2/HER2-overexpressing tumors using combinations of monoclonal antibodies: relevance of receptor endocytosis. Proc Natl Acad Sci USA 106(9):3294–3299